Hard diffractive $\eta_{c,b}$ hadroproduction at the LHC

Tichouk, Hao Sun ,[*] and Xuan Luo

Institute of Theoretical Physics, School of Physics, Dalian University of Technology,
No.2 Linggong Road, Dalian, Liaoning 116024, People's Republic of China

In this paper, we investigate the inclusive diffractive hadroproduction for η_c and η_b at the Large Hadron Collider (LHC) energies. Based on the nonrelativistic QCD factorization formalism and the resolved-Pomeron model for the quarkonium production mechanism, we estimate the rapidity, the momentum fraction loss dependence of the cross section. We give prediction ratios for single and central diffractive processes with respect to the nondiffractive process. These inclusive processes are sensitive to the gluon content of Pomeron for small x and Reggeon for large x, which is useful to study small and large-x physics and good to test different mechanisms for η_c and η_b production at the LHC. They also serve as the background to related exclusive processes; thus, they should be predicted. Our results demonstrate that the Reggeon contribution of diffractive processes can be sizable, even sometimes dominant over Pomeron, and that its study can be useful to better constrain the Reggeon parton content. The experimental study of Reggeon can be carried out in certain kinematic windows.

I. INTRODUCTION

The quarkonia production remains a topic of considerable theoretical and experimental interests in hadronic collisions at the Large Hadron Collider (LHC) and has attracted a lot of attention. It provides a valuable tool to test the ideas and methods of the QCD physics of bound states, such as effective field theories, lattice QCD, NRQCD, and so on [1]. Recently, the η_c hadroproduction cross section was measured by the LHCb experiments [2,3] in pp collisions which opened a window for the study of the pseudoscalar quarkonia production. This released experimental data provide a further important test for theories predicting the η_c hadroproduction cross sections polarization. The investigation of direct η_c hadroproduction at leading order (LO) in α_s within the NRQCD framework in the collinear factorization scheme has been carried out in Refs. [4–7] to describe the heavy quarkonium measurements. Besides, the QCD next-to-leading order (NLO) predictions of direct η_c hadroproduction have achieved good agreement with almost all the experimental measurements on quarkonia hadroproduction and clarified the ambiguity of the determination of the color octet long

distance matrix elements for J/ψ production [8–10]. However, the notorious J/ψ polarization in hadroproduction became rather puzzling for conventional nonrelativistic QCD (NRQCD) calculations at NLO in comparison to the world's data with transverse momenta up to 10 GeV [11]. Moreover, the examination of small or no polarization in the J/ψ meson prompt production [12] remains mysterious within the accessible theoretical framework [13]. The theory also lost its flexibility and made a prediction for η_c by a huge factor off the measured cross section with nonperturbative matrix elements fixed from fitting all other production data [14]. The general situation was even known as challenging [11]. In the investigation of the ground state, the η_c meson is still required so as to offer useful additional information on the long-distance matrix elements [15,16] and particularly, the heavy-quark spin-symmetry relation between the η_c and J/ψ matrix elements. Therefore, more studies on the η_c productions are being worked on or have been published; see, for example, the prompt η_c heavy quarkonium production that has been intensively examined in the transverse momentum dependent factorization with transverse momentum dependent distributions of on shell gluons [17], and the K_T-factorization scheme [18] along with the potential model in the transverse momentum space with off shell gluons [19].

It is not surprising that the η_c hadroproduction can be also used to study the soft interactions at the LHC, for example, through diffractive production modes in which no quantum numbers are exchanged between colliding particles at high energies. On top of that, it can be split into exclusive and inclusive event as displayed in Fig. 1.

[*]Corresponding author.
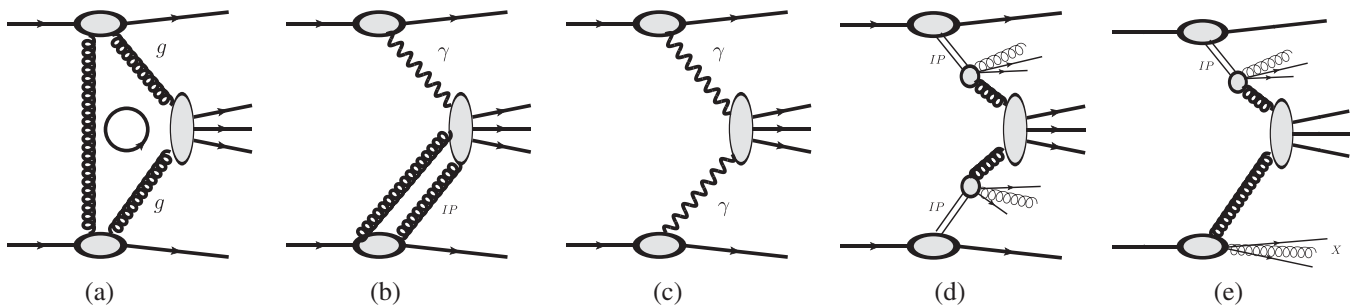haosun@mail.ustc.edu.cn, haosun@dlut.edu.cn

FIG. 1. The illustrative description of exclusive and inclusive processes.

Figure 1(a) describes schematically the exclusive diffraction via a two-gluon exchange between the two incoming protons. The soft pomeron is seen as a pair of gluons nonperturbatively coupled to the proton. One of the gluons is then coupled perturbatively to the hard process while the other one plays the role of a soft screening of color, allowing for diffraction to occur [20]. The exclusive diffraction events comprise the presence of the rapidity gaps, which separate the very intact forward outgoing protons from the centrally measured object produced alone. The intact forward outgoing protons are detected by forward hadron tagging detectors installed at a low scattering angle with respect to the beam axis near the central detector [21,22] after the exclusive diffractive collisions. The whole Pomeron energy is used to produce the diffractive state; i.e., there is no energy loss and Pomeron remnants [23]. The leading protons carry most of the beam particle momentum, and the full energy available is used in the interaction. The exclusive diffractive $\chi_{cJ}, \eta_c, J/\psi$ productions and so on have been studied in the Durham model with a tagged proton or antiproton [1,24–29] along with dedicated Monte Carlo codes [30]. The Figs. 1(b) and 1(c) describe other exclusive productions such as photon-Pomeron and photon-photon fusion, which are also very interesting. Notice that these purely exclusive production estimates can be useful to study the characteristics of the produced bound states or particles. However, their precise determinations lie in the consideration of the inclusive production [31], which serves as their important background. Here, in our present paper, we are concentrating on the inclusive diffractive production shown in Figs. 1(d) and 1(e).

As for the inclusive diffractive processes, they differ from their counterparts by smaller rapidity gaps, and the colliding Pomerons or Reggeons are composite systems made from quarks and gluons. There is also a presence of Pomeron or Reggeon remnants accompanied with soft QCD radiations. The presence of one intact forward hadron tagged in the final state and one large rapidity gap in the detector is called the single diffractive dissociation (SD). The central diffractive dissociation, double Pomeron or Reggeon exchange, or Pomeron-Reggeon cross exchange (DD) is characterized by two intact forward hadrons and two rapidies. The experimental diffractive studies [32–37] have particularly drawn attention toward the understanding of diffractive production due to the measurement of data samples released by the LHC. Theoretically, the inclusive diffractive processes have been studied in Regge theory (also named resolved-Pomeron model) in Refs. [38–41] and so on. Taking into consideration the perturbative QCD and the soft diffractive physics, some studies have shown and addressed the non-negligible Reggeon contribution [42,43]. In addition to the resolved-Pomeron model, existing models such as the Donnachie-Landshoff [20,44,45] model and the Bialas-Landshoff model [46] have also investigated diffractive production of particles.

In this paper, we have predicted the cross section for the inclusive single and double diffractive hadroproduction of η_c in proton-proton interactions in collinear momentum space in the NRQCD formalism with Regge theory. The nondiffractive hadroproduction (ND) has been estimated alongside diffractive ones. As said, on one hand, such a study can be the background of exclusive production which requires precise determination; on the other hand, they themselves are also sensitive to gluon content of Pomeron (Reggeon) whereas the Pomeron (Reggeon) themselves are sensitive to the gluon distribution in the proton. Thus, this kind of diffractive interaction is worth studying. Typically, we have also added Reggeon-Reggeon and Reggeon-Pomeron contributions, which have been usually ignored in other former calculations. We have concentrated on the η_c particle which is a pseudoscalar particle of an even charge parity. In this case, the dominant production mechanism is via the $gg \to \eta_c$ gluon-gluon fusion 2-1 process at the pole $z = 1$, where z is defined as $z = P_h \cdot P^{\eta_c}/P_h \cdot P_g$, where P_h, P_g, P^{η_c} are the four momenta of proton, gluon and η_c, respectively. The related diagrams are illustrated in Fig. 2. Notice that in the standard collinear factorization approach, there is a zero transverse momentum distribution for the final η_c, whereas the η_c production does possess transverse momentum distributions in the LHCb Collaboration measurement. We therefore comment that it may also be interesting to consider, for example, the $gg \to \eta_c + g$, $2 \to 2$ processes and study the kinematical
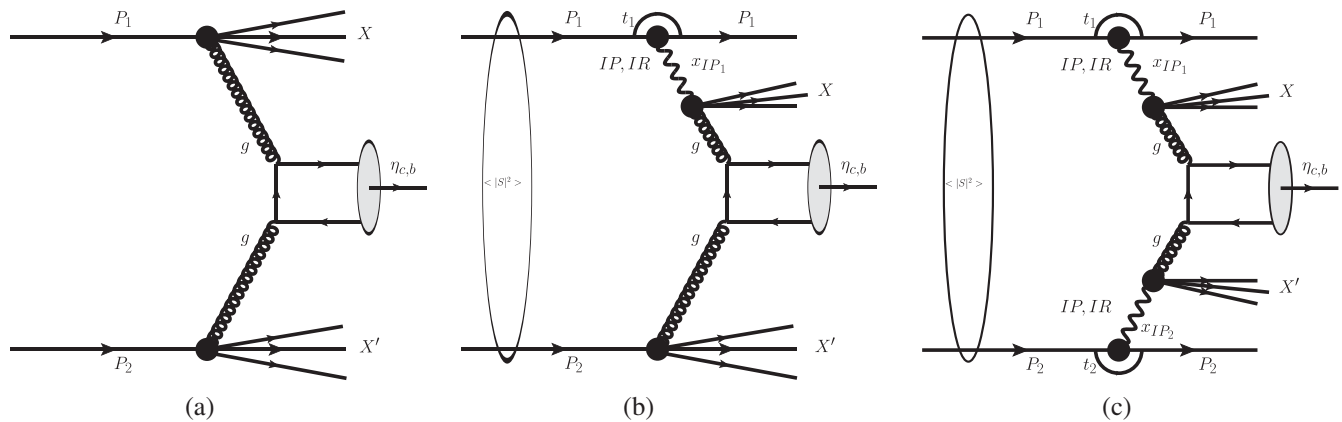
FIG. 2. Diagram representing single $\eta_{c,b}$ quarkonium hadroproduction in nondiiffraction (ND) (a), single diffraction (SD) (b), and double diffraction (DD) (c).

region $0 < z < 1$ and even go beyond the leading order approximation up to NLO to include the full region. In our future work, the transverse momentum will be also included in the perturbative QCD and the soft diffractive parts. Anyway, this paper is our first step towards future work that is in progress. The η_b production is also included in our work.

The paper is structured into three sections including the introduction in Sec. I. The detailed description of the hadron tagging devices and the formalism framework for the leading order cross section of η_c and η_b hadroproductions at the LHC are clearly described in Sec. II. The input parameters and discussed numerical results are shown in Sec. III. A summary is briefly given in Sec. IV.

II. FRAMEWORK OF THE CALCULATION TECHNOLOGY

A. Forward diffractive detectors

In SD and DD dissociations in a pp collision, the produced single η_c or η_b accompanied with a low-mass system are measured in the central detector. The initial incoming hadron, which is described by the different components of its wave function, can be absorbed during the diffractive scattering process. The final outgoing intact hadron can be just excited into a diffractive system and observed by forward detectors. The hadronic diffraction is where intact particles are excited into a hadronic system with a small invariant mass, much smaller than the collision energy. The experimental signature of this process is that all hadrons are produced at small angles. The central detectors can give the information to help the forward detector to identify diffractive and nondiffractive events [47]. In nondiffractive events, the color charge is exchanged between the interacting hadrons while the color singlet is exchanged in diffractive events [48]. The signal is to measure the exclusively produced heavy bound state in the central

detector, and the background is due to inclusive diffractive processes. The Pomeron or Reggeon remnants and QCD radiation are detected by the central detectors. There are two valuable detector characteristics of the diffractive processes, namely the existence of the intact initial hadron and large rapidity gap which goes together with it. The rapidity gap size and the location of them in the pseudorapidity phase space can be used to determine the type of the diffractions [49]. These rapidity gaps in the forward or backward rapidity regions, connect directly to the soft part of the events, and therefore, nonperturbative effects, on a long space-time scale.

The detectors possess the coverage necessary to measure forward rapidity gaps, Δy. Negative (positive) pseudorapidity or the large polar plane is referred to as left (right) side of the detector for $y < 0$ ($y > 0$). The pseudorapidity is often used experimentally instead of rapidity, since they are equal in the limit of a massless particle. These detectors try to measure both the cross sections and the kinematic properties of diffractive events at the LHC energies. The areas cover the range where protons are either both observed at 420 m (symmetric tagging) [50] or one is detected at 220 m and other at 420 m (asymmetric tagging). The forward tagging hadron detectors are characterized by their acceptance, resolution, and ability to measure the time-of-flight from the interaction point.

The transverse and longitudinal momenta defined relative to the beam axis, the azimuthal angle around the beam axis, and the pseudorapidity defined in terms of the polar angle θ with respect to the beam axis are kinematic variables for the diffractive processes. The coordinates (r, ϕ) are used in the plane transverse to the beam axis. The relationship between the observable Δy size and ξ_X is given as $\Delta y \simeq -\log(\xi_X)$ and $\Delta y \simeq \log(\xi_X \xi_{X'})$, where ξ_X is a function of the invariant mass of the whole diffractive final state, $M_X = \sqrt{\xi_X s}$ for single diffractive, $M_{XX'} = \sqrt{\xi_X \xi_{X'} s s'}$ for double diffractive, and the center of momentum

energy [51]. For proton tagging at the LHC, we have adopted a region of $0.0015 < \xi_1 < 0.5$, $0.1 < \xi_2 < 0.5$ for the CMS-TOTEM forward detector, and $0.015 < \xi_3 < 0.15$ for the AFP-ATLAS forward detector [21].

B. Cross section formulations

In the following section, we refer to the heavy quarkonia as η_c and η_b, whereas $h_1 h_2$ is symbolized by pp. The nondiffractive (ND), single diffractive (SD), and double diffractive (DD) hadron-hadron reactions are given as

$$
\begin{aligned}
\text{ND}:\ & h_1 h_2 \rightarrow \eta_{c,b} X \\
\text{SD}:\ & h_1 h_2 \rightarrow h_1 \otimes X + \eta_{c,b} + X' \\
\text{DD}:\ & h_1 h_2 \rightarrow h_1 \otimes X + \eta_{c,b} + X' \otimes h_2.
\end{aligned}
\tag{1}
$$

The total cross section of nondiffractive is given by the convolution of partonic cross section and gluon distribution functions of the incident particles for the correspondent process in gluon-gluon fusion and can be written as

$$
\sigma^{\text{ND}}(h_1 h_2 \rightarrow \eta_{c,b} X) = \int_0^1 \frac{dx_1}{x_1} \int_0^1 \frac{dx_2}{x_2} \sum_n \hat{\sigma}(gg \rightarrow Q\bar{Q}[n] + X) \langle 0 | \mathcal{O}_1^{\eta_{c,b}}[n] | 0 \rangle [\mathcal{F}_g(x_1, \mu^2) \mathcal{F}_g(x_2, \mu^2) + (h_1 \leftrightarrow h_2)], \quad (2)
$$

for a single diffractive process. The total cross section is written as

$$
\begin{aligned}
&\sigma^{\text{SD}}(h_1 h_2 \rightarrow h_1 \otimes X + \eta_{c,b} + X') \\
&= \langle |S|^2 \rangle \int_0^1 \frac{dx_1}{x_1} \int_0^1 \frac{dx_2}{x_2} \sum_n \hat{\sigma}(gg \rightarrow Q\bar{Q}[n] + X) \langle 0 | \mathcal{O}_1^{\eta_{c,b}}[n] | 0 \rangle [\mathcal{F}_g^D(x_1, \mu^2) \mathcal{F}_g(x_2, \mu^2) + (h_1 \leftrightarrow h_2)],
\end{aligned}
\tag{3}
$$

as for double diffractive process, the total cross section is formulated as

$$
\begin{aligned}
&\sigma^{\text{DD}}(h_1 h_2 \rightarrow h_1 \otimes X + \eta_{c,b} + h_2 \otimes X') \\
&= \langle |S|^2 \rangle \int_0^1 \frac{dx_1}{x_1} \int_0^1 \frac{dx_2}{x_2} \sum_n \hat{\sigma}(gg \rightarrow Q\bar{Q}[n] + X) \langle 0 | \mathcal{O}_1^{\eta_{c,b}}[n] | 0 \rangle [\mathcal{F}_g^D(x_1, \mu^2) \mathcal{F}_g^D(x_2, \mu^2) + (h_1 \leftrightarrow h_2)],
\end{aligned}
\tag{4}
$$

where $\langle 0 | \mathcal{O}_1^{\eta_{c,b}}[n] | 0 \rangle$ is the long-distance matrix element which describes the hadronization of the $Q\bar{Q}$ heavy pair into the physical observable quarkonium state η_c or η_b. The $\hat{\sigma}(gg \rightarrow Q\bar{Q}[n])$ denotes the short-distance cross sections for the partonic process $gg \rightarrow Q\bar{Q}[n]$, which is found by operating the covariant projection method [52,53]. The Fock state n are given as follows: ${}^1S_0^{[1]}$, ${}^1S_0^{[8]}$ for $gg \rightarrow Q\bar{Q}[n]$ partonic process [54]. The contribution of color singlet states for η_c and η_b quarkonium production is at leading power in velocity (v), while the color octet contribution to S-wave quarkonium production are power suppressed [55]. The $\mathcal{F}_g(x_i, \mu^2)$ and $\mathcal{F}_g^D(x_i, \mu^2)$ stand for the conventional integrated gluon parton distribution function (PDF) in the proton and their diffractive counterparts, respectively. x_i is the Bjorken variable defined as the momentum fractions of the hadron (proton) momentum carried by the gluons. $\langle |S|^2 \rangle$ is the gap survival probability or total factor. The partonic cross section is

$$
\hat{\sigma}(gg \rightarrow Q\bar{Q}[n]) = \frac{\pi}{M_{\eta_{c,b}}^2} \delta(\hat{s} - M_{\eta_{c,b}}^2) \overline{\sum} |\mathcal{A}_{S,L}|^2 \quad (5)
$$

with the matrix element squared given by [56–58]

$$
\begin{aligned}
\overline{\sum} |\mathcal{A}_{S,L}|^2 &= \frac{2}{9} \frac{\pi^2 \alpha_s^2}{M_{\eta_{c,b}}} \langle 0 | \mathcal{O}_1^{\eta_{c,b}}({}^1S_0) | 0 \rangle \\
&+ \frac{5}{12} \frac{\pi^2 \alpha_s^2}{M_{\eta_{c,b}}} \langle 0 | \mathcal{O}_8^{\eta_{c,b}}({}^1S_0) | 0 \rangle,
\end{aligned}
\tag{6}
$$

and the colliding energy is written as $\hat{s} = x_1 x_2 s$.

C. Gap survival probability in diffractive processes

The gap survival probability [59] is characterized by the presence of additional soft partonic interactions and new particles in gap rapidity. It can be described by additional soft incoming or outgoing proton-proton rescatterings with multi-Pomerons exchanged (eikonal factor), by the interaction of an incoming or outgoing proton with intermediate partons (enhanced factor), by gluon radiation from annihilation of two energetic colored particles called hard QCD bremsstrahlung (Sudakov factor), and by the change of the forward intact proton momentum (migration).

The enhanced and Sudakov factors as well as the migration are neglected in the collinear approximation, where the transverse momenta of intermediate partons and screening gluon are not taken into consideration and the incoming proton and outgoing intact forward proton have almost the same direction. The eikonal gap survival

probability has been evaluated as $\langle|S|^2\rangle$ [42,60,61] and reads

$$\langle|S|^2\rangle_{pp} = \frac{B_1}{B_\mathbb{P}}\left(\frac{\sigma_{pp}^{tot}(s)}{2\pi B_1}\right)^{-B_1/B_\mathbb{P}} \gamma\left(B_1/B_\mathbb{P}, \frac{\sigma_{pp}^{tot}(s)}{2\pi B_1}\right), \quad (7)$$

where γ is the incomplete gamma function, $\sqrt{s} = 13$ TeV, $B_1 = \frac{B_0}{2} + \frac{\alpha'}{2}\ln(\frac{s}{s_0})$ [62,63], $s_0 = 1$ GeV^2 for two channel model [64], $B_0 = 10$ GeV^{-2}, $\alpha' = 0.25$ GeV^{-2}, $B_2 = \frac{1}{2Q_0^2} + \frac{B_1}{4}$. The chosen total pp cross section is parametrized by the optical theorem in one way as $\sigma_{pp}^{tot}(s) = 33.73 + 0.2838\ln^2(s) + 13.67\ s^{-0.412} - 7.77\ s^{-0.5626}$ mb [65,66] and in another way as $\sigma_{pp}^{tot}(s) = 69.3286 + 12.6800\ln(\sqrt{s}) + 1.2273\ln^2(\sqrt{s})$ [67]. Thus, its computed value is $\langle|S|^2\rangle_{pp} = 0.09(0.03)$ for the LHC energy. The approximative formula is also given as [42,60,61]

$$\langle|S|^2\rangle_{pp} = \frac{a}{b + \ln(\sqrt{s/s_0})}, \quad (8)$$

with $a = 0.126$, $b = -4.688$, and this approximative value is $\langle|S|^2\rangle_{pp} = 0.03$ [68]. Those additional soft interactions from the eikonal factor can destroy the diffractive signature [69] and the Regge factorization is known to be violated in the treatment of diffractive interactions in hadronic collisions. The gap survival probability relies on the specific collision, the cuts prescribed in the experiment, and stands for the last element of the resolved-Pomeron model. A variety of attempts have been carried out to estimate those probabilities [70–72]; however, the actual values are rather uncertain. The selected value can be regarded a lower limit given the recent available experimental results [73,74].

D. The Pomeron and Reggeon parton distribution functions

As stated by the so-called proton-vertex factorization or the resolved Pomeron model [38], the collinear diffractive gluon, $g_p^D(x_g, \mu_f^2, x_\mathbb{P})$ is defined as a convolution of the Pomeron (Reggeon) flux emitted by the proton, $f_{\mathbb{P},\mathbb{R}}^h(x_\mathbb{P})$, and the gluon distribution in the Pomeron (Reggeon), $g^{\mathbb{P},\mathbb{R}}(\beta, Q^2)$, where $\beta(= \frac{x_1}{x_\mathbb{P}})$ is the longitudinal momentum fraction carried by the partons inside the Pomeron. The Reggeon contribution is ignored in the hard diffraction calculations of different final states in most cases. The Reggeon contribution is treated as an exchange of a quark and antiquark pair, and the parton content of the Reggeon is obtained from the pion structure function [75]. The difference between the two contributions exists in the $x_\mathbb{P}$ and t dependence of their fluxes, where the Reggeon exchange is mostly significant at high $x_\mathbb{P}$, remarkably for $x_\mathbb{P} > 0.1$. $x_\mathbb{P}$ stands also for ξ. The Reggeon shape of the t distribution is also different, showing a less steep decrease than in the Pomeron case. Nevertheless, as shown in Ref. [68], this

contribution is significant in some regions of the phase space and needs to obtain a good description of the data. The collinear diffractive gluon distribution of the proton at low β and large $x_\mathbb{P}$ [76,77] is formulated by

$$g_p^D(x_g, Q^2, x_\mathbb{P}) = \int_{x_g}^1 \frac{dx_\mathbb{P}}{x_\mathbb{P}} f_\mathbb{P}^p(x_\mathbb{P}) g^\mathbb{P}\left(\frac{x_g}{x_\mathbb{P}}, Q^2\right)$$
$$+ n_\mathbb{R} \int_{x_g}^1 \frac{dx_\mathbb{P}}{x_\mathbb{P}} f_\mathbb{R}^p(x_\mathbb{P}) g^\mathbb{R}\left(\frac{x_g}{x_\mathbb{P}}, Q^2\right), \quad (9)$$

and the Pomeron and Reggeon fluxes are literally expressed by

$$f_{\mathbb{P},\mathbb{R}}^p(x_\mathbb{P}) = \int_{t_{min}}^{t_{max}} dt f_{\mathbb{P},\mathbb{R}/p}(x_\mathbb{P}, t) = \int_{t_{min}}^{t_{max}} dt \frac{A_{\mathbb{P},\mathbb{R}} e^{B_{\mathbb{P},\mathbb{R}}t}}{x_\mathbb{P}^{2\alpha_{\mathbb{P},\mathbb{R}}(t)-1}},$$
$$(10)$$

where the variables, t_{min} and t_{max}, are kinematically fixed limits. The Pomeron (Reggeon) flux factor is stimulated by Regge theory, where the Pomeron (Reggeon) trajectory is linearly supposed to be, $\alpha_{\mathbb{P},\mathbb{R}}(t) = \alpha_{\mathbb{P},\mathbb{R}}(0) + \alpha'_{\mathbb{P},\mathbb{R}}t$, and the parameters $B_{\mathbb{P},\mathbb{R}}$, $\alpha'_{\mathbb{P},\mathbb{R}}(t)$ and their uncertainties are taken from fits to H1 data [75]. The slope of the Pomeron (Reggeon) flux is $B_{\mathbb{P},\mathbb{R}} = 5.5^{-2.0}_{+0.7}(1.6^{-1.6}_{+0.4})$ GeV^{-2}, the Regge trajectory of the Pomeron (Reggeon) $\alpha_{\mathbb{P},\mathbb{R}}(t) = \alpha_{\mathbb{P},\mathbb{R}}(0) + \alpha'_{\mathbb{P},\mathbb{R}}(t)$ with $\alpha_{\mathbb{P},\mathbb{R}}(0) = 1.118 \pm 0.008(0.50 \pm 0.10)$ and $\alpha'_{\mathbb{P},\mathbb{R}} = 0.06^{+0.19}_{-0.06}$ GeV$^{-2}(0.3^{+0.6}_{-0.3}$ GeV$^{-2})$. The t integration limits are $t_{max} = -m_p^2 x_\mathbb{P}^2/(1-x_\mathbb{P})$ ($m_p = 0.93827231$ GeV symbolizes the proton mass) and $t_{min} = -1$ GeV^2. Lastly, the normalization factor $A_{\mathbb{P},\mathbb{R}} = 1.7101(1705.0)$ is selected such that $x_\mathbb{P} \times \int_{t_{min}}^{t_{max}} dt f_{\mathbb{P},\mathbb{R}/p}(x_\mathbb{P},t) = 1$ at $x_\mathbb{P} = 0.003$ and $n_\mathbb{R} = (1.7 \pm 0.4) \times 10^{-3}$. The $f_{\mathbb{P},\mathbb{R}}^p(x_\mathbb{P})$ is the Pomeron (Reggeon) flux factor which describes the emission rate of Pomeron (Reggeon) by the hadron (p) and represents the probability that a Pomeron with particular values of $(x_\mathbb{P}; t)$ couples to the hadron. A certain fraction of the pomeron energy is only available for the hard collision, and the rest is carried away by a remnant or spectator jet. On every occasion, a colored parton (gluon) is pulled out of a color-singlet object, Pomeron. The Pomeron structure is well restricted by the fits, fit A and fit B, which evidently reveal that its parton content is gluon dominated. Contrariwise, the HERA data do not restrain the parton distribution function of Reggeon which is therefore needed in order to get a quantitative description of the high-$x_\mathbb{P}$ measurements. Consequently, measurements at the LHC will permit us to examine the validity of this supposition.

III. NUMERICAL RESULTS AND DISCUSSION

In the following part, we discuss the numerical results of the inclusive and diffractive hadroproduction of $\eta_{c,b}$ by

TABLE I. The total cross section (μb) for η_c hadroproduction at the LHC with forward detector acceptances.

Process		ξ_i		
		$0.0015 < \xi_1 < 0.5$	$0.1 < \xi_2 < 0.5$	$0.015 < \xi_3 < 0.15$
SD	$\mathbb{P}$p	11.8	3.84	5.72
	$\mathbb{R}$p	20.6	18.6	3.72
	Total	32.4	22.4	9.44
DD	$\mathbb{P}\mathbb{P}$	4.74×10^{-1}	1.74×10^{-2}	9.32×10^{-2}
	$\mathbb{P}\mathbb{R} + \mathbb{R}\mathbb{P}$	2.25	6.14×10^{-1}	2.16×10^{-1}
	$\mathbb{R}\mathbb{R}$	1.79	1.45	6.06×10^{-2}
	Total	4.51	2.08	3.70×10^{-1}
ND	gg		2050.07	

using some physical parameters such as the masses of the heavy quarks chosen as $m_c = 1.45$ GeV and $m_b = 4.75$ GeV. The mass of $\eta_{c,b}$ is literally put at $M_{\eta_{c,b}} = 2m_{c,b}$. The colliding energy used in this paper is $\sqrt{s} = 13$ TeV for pp. For the unpolarized distribution function of a gluon from the proton, we adopt the leading-order set of the MSTW2008 parametrization [78]. The 2006 H1 proton diffractive PDFs (fit A) are used for the Pomeron densities inside the proton [75,77], which are probed at the factorization hard scale ($\mu = Q$) chosen as $\mu = m_T^{\eta_{c,b}}$, where $m_T^{\eta_{c,b}} = M_{\eta_{c,b}}$ is the $\eta_{c,b}$ transverse mass. Numerical calculations are carried out by an in-house Monte Carlo generator. The choice of the long distance matrix elements for $\eta_{c,b}$ is taken from [57,79,80] and valued to $\langle 0|\mathcal{O}_1^{\eta_c}(^1S_0)|0\rangle = 0.44$ GeV^3, $\langle 0|\mathcal{O}_8^{\eta_c}(^1S_0)|0\rangle = 0.00056$ GeV^3, $\langle 0|\mathcal{O}_1^{\eta_b}(^1S_0)|0\rangle = 3.63333$ GeV^3, and $\langle 0|\mathcal{O}_8^{\eta_b}(^1S_0)|0\rangle = 0.0159$ GeV^3.

A. The cross sections

In Table I, the total cross section predictions of η_c hadroproduction in ND, SD, and DD processes are displayed for three different forward detector acceptances at the distinct ranges, $0.0015 < \xi_1 < 0.5$, $0.1 < \xi_2 < 0.5$, and $0.015 < \xi_3 < 0.15$. In the single diffraction dissociation, we have noticed that the $\mathbb{R}$p contributions are more substantial than that of $\mathbb{P}$p contributions for $\xi_{1,2}$, whereas the large contribution to the total cross section for ξ_3 hails from the $\mathbb{P}$p interactions. That means that the Reggeon contribution should be taken into consideration for some Reggeon longitudinal momentum fraction ranges at the LHC experiments and should not be neglected particularly for $\xi_{1,2}$. As for the double diffraction dissociation, $\mathbb{R}\mathbb{R}$ and $\mathbb{P}\mathbb{R} + \mathbb{P}\mathbb{R}$ interactions provide more contributions to the total cross section of η_c for $\xi_{1,2}$. In the case of ξ_3, the large contribution to the total cross section comes from the $\mathbb{P}\mathbb{R} + \mathbb{P}\mathbb{R}$ cross exchange interactions. Reggeon contributions are still yet important for some same forward detector acceptances like in the SD process. The $\mathbb{R}\mathbb{P}$ and $\mathbb{R}\mathbb{R}$ interactions should play a non-negligible contribution to the η_c hadroproduction for Pomeron/Reggeon longitudinal momentum

fraction range, as far as the $\xi_{1,2}$ are concerned. We have also seen, the nondiffractive prediction is a factor 10^2 (10^3), 10^2 (10^3), and 10^3 (10^4) larger than that of a SD (DD) prediction for $0.0015 < \xi_1 < 0.5$, $0.1 < \xi_2 < 0.5$ and $0.015 < \xi_3 < 0.15$, respectively. The total cross sections made the approximation of neglecting the Reggeon contributions even more problematical. Reggeon can be more of a contribution than that of the Pomeron to a total quarkonium cross section in some kinematical ranges where it clearly dominates, and Reggeon can be experimentally isolated.

In Table II, we have also estimated the η_b cross section for ND, SD, and DD dissociations for ξ_1 only where the Reggeon contribution to the cross section is little bit sizable. The nondiffractive prediction is a factor 10^2 (10^3) larger than the SD (DD) prediction of η_b hadroproduction for $0.0015 < \xi_1 < 0.5$. The nondiffractive, single, and double diffractive cross section of η_c is a factor 10^2 larger than that of η_b due to its small mass.

The diffractive production rates for η_c and η_b in pp interactions assumes the design integrated luminosities $\mathcal{L}_{LHC}^{pp} = 10^4$ μb^{-1} s^{-1} and run times (T = 10 s) [81]. The production rate in ND, SD, and DD processes are more sensitive to proton momentum loss, $0.0015 < \xi_1 < 0.5$, due to its considerable Reggeon event numbers.

TABLE II. The total cross section (μb) for the η_b hadroproduction at LHC for forward detector acceptances, $0.0015 < \xi_1 < 0.5$.

Process		ξ_i
		$0.0015 < \xi_1 < 0.5$
SD	$\mathbb{P}$p	1.66×10^{-1}
	$\mathbb{R}$p	2.39×10^{-1}
	Total	4.05×10^{-1}
DD	$\mathbb{P}\mathbb{P}$	9.31×10^{-3}
	$\mathbb{P}\mathbb{R} + \mathbb{R}\mathbb{P}$	2.82×10^{-2}
	$\mathbb{R}\mathbb{R}$	1.82×10^{-2}
	Total	5.57×10^{-2}
ND	gg	24.68

TABLE III. The uncertainties for the η_c and η_b hadroproductions at LHC for forward detector acceptances, $0.0015 < \xi_1 < 0.5$.

Process			ξ_i
			$0.0015 < \xi_1 < 0.5$
η_c	SD	$\mathbb{P}$p	[10.12; 15.46]
		Total	[30.73; 36.07]
	DD	$\mathbb{P}\mathbb{P}$	$[4.10 \times 10^{-1}; 5.90 \times 10^{-1}]$
		$\mathbb{P}\mathbb{R} + \mathbb{R}\mathbb{P}$	[1.94; 2.88]
		Total	[4.14; 5.26]
η_b	SD	$\mathbb{P}$p	$[1.53 \times 10^{-1}; 1.87 \times 10^{-1}]$
		Total	$[3.92 \times 10^{-1}; 4.27 \times 10^{-1}]$
	DD	$\mathbb{P}\mathbb{P}$	$[8.18 \times 10^{-3}; 1.11 \times 10^{-2}]$
		$\mathbb{P}\mathbb{R} + \mathbb{R}\mathbb{P}$	$[2.56 \times 10^{-2}; 3.23 \times 10^{-2}]$
		Total	$[5.21 \times 10^{-2}; 6.16 \times 10^{-2}]$

TABLE IV. The ratios for η_c and η_b (in parentheses) hadroproductions at LHC for different forward detector acceptances.

$R_i \backslash \xi_i$	$0.0015 < \xi_1 < 0.5$	$0.1 < \xi_2 < 0.5$	$0.015 < \xi_3 < 0.15$
R_1	1.58% (1.64%)	1.09%	0.46%
R_2	0.22% (0.22%)	0.10%	0.02%
R_3	13.92% (13.75%)	9.28%	3.92%

The predictions are influenced by large theoretical errors as mentioned above. Those uncertainties can be suitably lessened by taking into account the ratio R_i of diffractive to nondiffractive cross sections and double diffractive to single diffractive cross sections,

$$R_1 = \frac{\sigma_{SD}}{\sigma_{ND}}; \qquad R_2 = \frac{\sigma_{DD}}{\sigma_{ND}}; \qquad R_3 = \frac{\sigma_{DD}}{\sigma_{SD}}, \qquad (11)$$

which give the advantage to reduce experimentally systematic errors. The ratios have been measured in a range of final states at the Tevatron, and certain stable behaviors with a value near 1% have been displayed [35–37]. We have presented these ratios of cross sections of η_c and η_b in Table IV. Our η_c ratio results have indicated that the single diffractive dissociation to nondiffractive process provides the leading order estimate of 1.58%, 1.09%, and 0.46% for $0.0015 < \xi_1 < 0.5, 0.1 < \xi_2 < 0.5$, and $0.015 < \xi_3 < 0.15$, respectively. As for η_b, the ration is of 1.64% for $0.0015 < \xi_1 < 0.5$.

The nondiffractive event rate keeps the same order of magnitude larger than SD and DD as for η_b and η_c cross section predictions. The LHC capabilities should be utilized in order to constrain it better and improve the theoretical event rate predictions of the various Pomeron/Reggeon longitudinal momentum fraction range studies.

The estimate of uncertainty in inclusive diffractive cross section predictions arises from many sources. Firstly, it can be evaluated from different choices of the heavy quark masses, the long distance elements, the factorization scale, or renormalization scale [82]. Secondly, the uncertainty can come from the gap survival probability, which gives maybe the largest uncertainty of about ±50% [83] or around 30% [42] in the overall production rate. The obtained results can be multiplied by a factor of 4 at CMS collider [73]. Thirdly, the error can be computed by the choice of two different diffractive PDF fits, H1 2006 dPDF fit A and H1 2006 dPDF fit B. The results are found slightly different between these two fits. Fourthly, the gluon density at high β is however poorly known, and the uncertainty is of the order of 25%. This high β region is of particular interest for the LHC since it represents, for example, a direct background to the search for exclusive events [84]. This uncertainty takes into account the uncertainty of QCD fits at high β and is related only to the gluon density from Pomeron $g^{\mathbb{P}}(\frac{x_g}{x_{\mathbb{P}}}, Q^2)$, which is multiplied by an uncertainty factor $(1 - \beta)^\nu$ with $\nu = -0.5$ or 0.5 [40,85]. It is evaluated in Table III for total SD and DD cross sections of η_c and η_b diffractive hadroproductions in pp collisions for $0.0015 < \xi_1 < 0.5$. Fifthly, it is also worth mentioning that the uncertainty range of the Reggeon contribution is unknown in literature. Sixthly, there are uncertainties which hail from the infrared region, where the gluon distribution is not well understood as well as the uncertainty in the gluon distribution itself. And finally, it has been noted that in the higher-order QCD, radiative corrections cause additional uncertainties [1].

B. Double diffraction distributions

In Fig. 3, we exhibit our predictions of y^{η_c} and y^{η_b} distributions for double diffractive hadroproduction in pp collisions at the LHC energies for three different forward detector acceptances. The incident protons, which are sources of Pomeron and Reggeon, remain undissociated in the final state. The forward and backward detectors are placed at small angles to observe those intact protons while the central detector is located to detect the η_c or η_b and other particles. Protons can either emit gluons, Pomeron, or Reggeon. When the colliding protons emit gluons, the emerging protons remain dissociated. There is also a case where one proton emits a Reggeon and the other proton emits a Pomeron. We can observe that in these differently aforementioned collisions, the y^{η_c} and y^{η_b} distributions are symmetric with respect to the midrapidity $y^{\eta_c} = 0$ and $y^{\eta_b} = 0$, where η_c, η_b, and other unknown particles (X and X′) are detected. This symmetry is due to equal forward and backward rapidities, where the colliding protons emits either the same particles such as a gluon, Pomeron, and Reggeon, or different particles (Reggeon from one proton and Pomeron from another proton). The Pomeron and Reggeon behaving like composite particles will emit in their turns diffractive gluons for the hard interactions. The total Pomeron-Reggeon, Reggeon-Pomeron, and Reggeon-Reggeon contribution also shows a symmetric distribution.
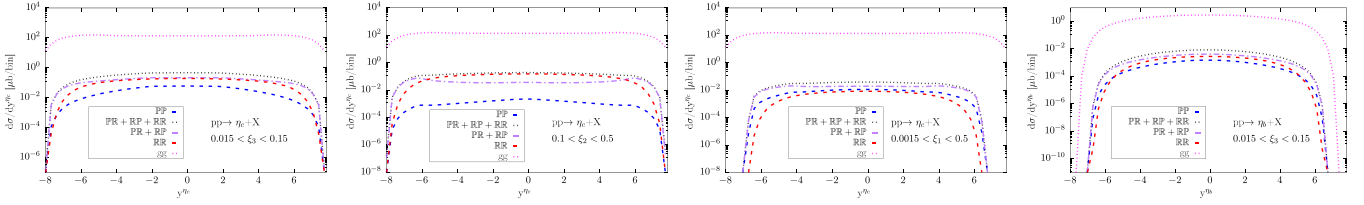
FIG. 3. The y^{η_c} and y^{η_b} distributions for the $\mathbb{P}\mathbb{P}$ (blue dashed line), $\mathbb{P}\mathbb{P} + \mathbb{P}\mathbb{R} + \mathbb{R}\mathbb{P} + \mathbb{R}\mathbb{R}$ (black dotted line), $\mathbb{P}\mathbb{R} + \mathbb{R}\mathbb{P}$ (purple dash dotted line), $\mathbb{R}\mathbb{R}$ (red dashed line), and gg (magenta dotted line) in DD processes.

y^{η_c} and y^{η_b} distributions for a nondiffractive process largely predominate over the diffractive processes. The y^{η_c} distributions from Pomeron-Pomeron (Reggeon-Reggeon) interactions are the lowest for the forward acceptance detector $0.0015 < \xi_1 < 0.5$ and $0.1 < \xi_2 < 0.5$ $(0.015 < \xi_3 < 0.15)$. The Reggeon contribution is sensitive to forward detector acceptances such as $\xi_{1,2}$. It becomes clearly dominant for $0.0015 < \xi_1 < 0.5$. The y^{η_c} and y^{η_b} distributions for the double diffractive dissociation have maximums concentrated at midrapidities. The contribution of Reggeon-Reggeon and Reggeon-Pomeron interactions can not be disregarded over the Pomeron-Pomeron interaction in some regions where the $\xi_{1,2}$-cuts are applied. The y^{η_b} distributions are more significant than that of the y^{η_c} distribution ones for the three forward detector acceptances. By measuring these distributions, we should be able to investigate the Reggeon contribution at the LHC data.

In Fig. 4, we have plotted $x^{\eta_c}_{\mathbb{P}_1}$, $x^{\eta_c}_{\mathbb{P}_2}$, $x^{\eta_c}_{\mathbb{P}_1}$, and $x^{\eta_c}_{\mathbb{P}_2}$ distributions for DD processes. We have noticed the distributions of two colliding protons in DD process are slightly similar because their proton momentum loss are closely equal. The Reggeon-Reggeon contribution increases for low range of $x_{\mathbb{P}_1}$ and $x_{\mathbb{P}_2}$. It becomes flat for large $x_{\mathbb{P}_1}$ and $x_{\mathbb{P}_2}$ ranges, where its contribution is non-negligible. The Pomeron-Pomeron contribution continuously decreases for low and large ranges of $x_{\mathbb{P}_1}$ and $x_{\mathbb{P}_2}$,

meanwhile the Pomeron-Reggeon contribution decreases for low range and turns out to be flat for a large range. The Reggeon-Reggeon contribution is useful at large $x_{\mathbb{P}_1}$ and $x_{\mathbb{P}_2}$ over the Pomeron-Pomeron contribution one and can not be neglected. Reggeon contributions dominate for large values of proton momentum loss while the Pomeron exchange is still dominant for small values [68]. The Reggeon contribution sensitivity can be increased near the edge of the proton forward detector acceptance, and it becomes evidently dominant.

In Fig. 5, we have presented the β_1 and β_2 distributions of η_c for three different forward detector acceptances $(\xi_{1,2,3})$. We have also plotted for one forward detector acceptance (ξ_3) for η_b. We realize that all the contributions decrease, become flat, and decrease again, except for the Reggeon-Reggeon contribution, where the decrease is spread over all ranges of β_1 and β_2. The Reggeon-Reggeon contribution is dominant for small β_1 and β_2 over the Pomeron-Pomeron contribution. They become comparable for very small β_1 and β_2. However, we also notice that the Pomeron-Pomeron contribution surpasses that of Reggeon-Reggeon one for large β_1 and β_2. For $0.015 < \xi_3 < 0.15$ $(0.0015 < \xi_1 < 0.5)$, the Reggeon-Reggeon contribution is dominated by the Pomeron-Pomeron one for η_c (η_b) for small β_1 and β_2. When β_1 and β_2 tend to very small values, the Reggeon-Reggeon contribution is comparable to the Pomeron-Pomeron
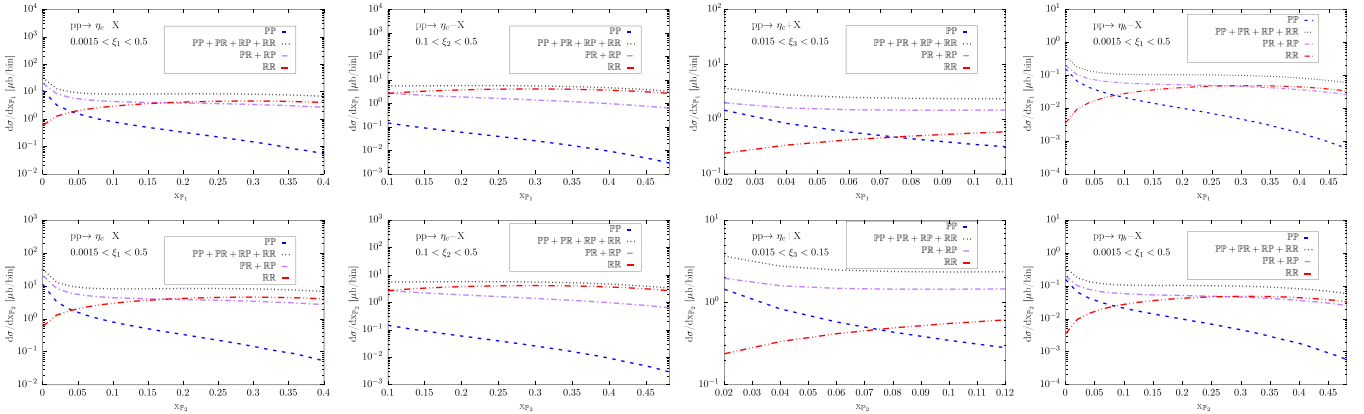
FIG. 4. The $x^{\eta_c}_{\mathbb{P}_1}$ and $x^{\eta_c}_{\mathbb{P}_2}$ distributions (top panel) and, $x^{\eta_c}_{\mathbb{P}_2}$ and $x^{\eta_c}_{\mathbb{P}_1}$ distributions (bottom panel) for the $\mathbb{P}\mathbb{P}$ (blue dashed line), $\mathbb{P}\mathbb{P} + \mathbb{P}\mathbb{R} + \mathbb{R}\mathbb{P} + \mathbb{R}\mathbb{R}$ (black dotted line), $\mathbb{P}\mathbb{R} + \mathbb{R}\mathbb{P}$ (purple dash dotted line), and $\mathbb{R}\mathbb{R}$ (red dashed line) in DD processes.
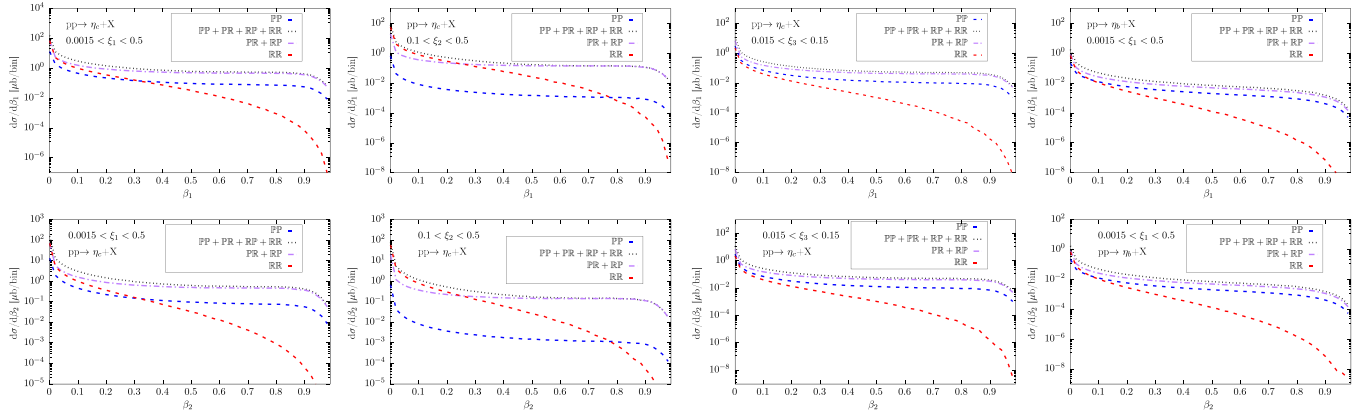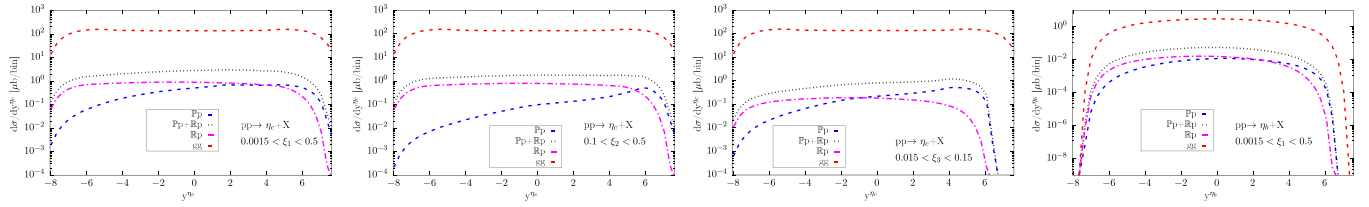
FIG. 5.   The β_1 distributions (top panel) and β_2 distributions (bottom panel) for the $\mathbb{PP}$ (blue dashed line), $\mathbb{PP} + \mathbb{PR} + \mathbb{RP} + \mathbb{RR}$ (black dotted line), $\mathbb{PR} + \mathbb{RP}$ (purple dash dotted line), and $\mathbb{RR}$ (red dashed line) in DD processes.

FIG. 6.   The y^{η_c} and y^{η_b} distributions for the $\mathbb{P}p$ (blue dashed line), $\mathbb{P}p + \mathbb{R}p$ (black dotted line), $\mathbb{R}p$ (purple dash dotted line), and gg (red dotted line) in SD processes.

contribution. The behavior of these plots is related to $\beta_1 = \frac{x_1}{x_{\mathbb{P}_1}}$ and $\beta_2 = \frac{x_2}{x_{\mathbb{P}_2}}$.

C. Single diffraction distributions

In Fig. 6, we have the exhibition of the y^{η_c} distributions in SD dissociation for three different forward detector acceptances. In this case, one of the two protons emits a gluon and the second proton emits Pomeron or Reggeon with a small squared momentum transfer. What is more, Pomeron or Reggeon can emit also a diffractive gluon before hard scattering. Afterward, the gluon and diffractive gluon go into hard collision. The proton emitting the Pomeron or Reggeon remains intact by turning into the excited one and is detected by the forward and backward detectors, while the proton emitting gluons only dissociates into a new system called remnant (X, X') observed by

the central detectors. We can see that the y^{η_c} distributions are asymmetric with respect to the midrapidity $y^{\eta_c} = 0$ for $\mathbb{P}p$ and $\mathbb{R}p$ contributions. This asymmetry is caused by the inequality in forward and backward rapidities. y^{η_c} distributions for nondiffractive process, where the two protons emit gluons only, largely dominate over the diffractive processes. Its distribution is symmetric. The y^{η_c} distributions from Reggeon interactions dominate over the Pomeron ones for small values of rapidities. Nevertheless, the Pomeron contribution is important for large values of rapidities. The y^{η_b} distribution is displayed for $0.0015 < \xi_1 < 0.5$. Its distribution is more important than that of y^{η_c}. The y^{η_c} and y^{η_b} distributions for the single diffractive dissociation have maximums shifted to forward and backward rapidities with respect to the nondiffractive case. The constraint on Reggeon distribution at LHC should enhance the theoretical predictions for η_c and η_b.
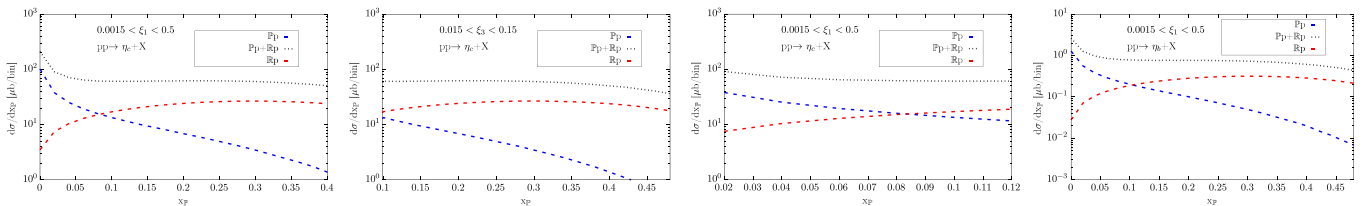

FIG. 7.   The $x_{\mathbb{P}}^{\eta_c}$ and $x_{\mathbb{P}}^{\eta_c}$ distributions for the $\mathbb{P}p$ (blue dashed line), $\mathbb{P}p + \mathbb{R}p$ (black dotted line), and $\mathbb{R}p$ (red dash dotted line) in SD processes.
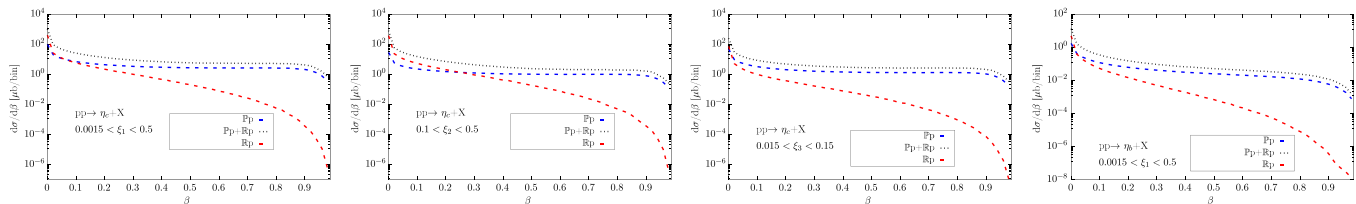
FIG. 8. The β distributions for the $\mathbb{P}p$ (blue dashed line), $\mathbb{P}p + \mathbb{R}p$ (black dotted line), and $\mathbb{R}p$ (red dash dotted line) in SD processes.

In Fig. 7, we have plotted the $x_{\mathbb{P}}^{\eta_c}$ and $x_{\mathbb{P}}^{\eta_c}$ distributions for SD processes. The $\mathbb{R}p$ contribution increases for the low range of $x_{\mathbb{P}}$. It becomes slightly flat for the large range, where its contribution is non-negligible. The $\mathbb{P}p$ contribution always decreases for low and large ranges of $x_{\mathbb{P}}$. The $\mathbb{R}p$ contributions dominate for large values of proton momentum loss while the $\mathbb{P}p$ is still dominant at small values [68]. The Reggeon contribution sensitivity can be increased near the edge of the proton forward detector acceptance, and it becomes evidently dominant.

The presentation of the β distributions of η_c and η_b of three different cuts for forward detector acceptance is given in Fig. 8 for SD dissociation. The decreasing and fattening of the all contributions are observed on plots. The $\mathbb{R}p$ contribution shows a decreasing behavior along with β and is dominant for small β over the $\mathbb{P}p$ contribution. Nonetheless, we also notice that the $\mathbb{P}p$ contribution overpasses that of the $\mathbb{R}p$ one for large β, and they become comparable for very small β. For the $0.015 < \xi_3 < 0.15$ $(0.0015 < \xi_1 < 0.5)$, the $\mathbb{R}p$ contribution is small compared to that of $\mathbb{P}p$ for η_c (η_b) for large β, and they become comparable for very small β.

Our results show that η_c and η_b hadroproduction in SD and DD processes at the LHC could be used to study the Reggeon contribution, since a kinematic window of dominance has been identified which could be used experimentally to isolate and constrain it. Our values are in agreement with the prediction that single diffractive cross sections should be approximately 10 times greater than that in the

double diffractive case [68,86]. We have found that Reggeon exchanges contribute much more in some range of forward detector acceptance and can almost never be completely disregarded. For large values of $x_{\mathbb{P}}$ and small values of β but still within the detector acceptances, processes involving Reggeons can even dominate over the double-Pomeron exchange. For very small β, Reggeon and Pomeron exchanges are comparable.

IV. SUMMARY AND CONCLUSION

In this work, we calculate the hadroproduction of η_c and η_b via single diffractive, double diffractive, and nondiffractive processes at the LHC $\sqrt{s} = 13$ TeV energies. Considering the NRQCD formalism along with the resolved-Pomeron model, we predict the total cross sections, the differential, and the production rates for these processes. Our results demonstrate that the contribution of Reggeon are non-negligible orders of magnitude for certain forward detector acceptances, and therefore, this study can be useful to better constrain the Reggeon parton content and correct the experimental model.

ACKNOWLEDGMENTS

[1] L. A. Harland-Lang, V. A. Khoze, M. G. Ryskin, and W. J. Stirling, Eur. Phys. J. C **65**, 433 (2010).

[2] R. Aaij et al. (LHCb Collaboration), Eur. Phys. J. C **75**, 311 (2015).

[3] R. Aaij et al. (LHCb Collaboration), Eur. Phys. J. C **80**, 191 (2020).

[4] S. S. Biswal and K. Sridhar, J. Phys. G **39**, 015008 (2012).

[5] A. K. Likhoded, A. V. Luchinsky, and S. V. Poslavsky, Mod. Phys. Lett. A **30**, 1550032 (2015).

[6] P. Mathews, P. Poulose, and K. Sridhar, Phys. Lett. B **438**, 336 (1998); **479(E)**, 343 (1999).

[7] L.-K. Hao, F. Yuan, and K.-T. Chao, Phys. Rev. Lett. **83**, 4490 (1999).

[8] H.-F. Zhang, Z. Sun, W.-L. Sang, and R. Li, Phys. Rev. Lett. **114**, 092006 (2015).

[9] Y. Feng, J. He, J.-P. Lansberg, H.-S. Shao, A. Usachov, and H.-F. Zhang, Nucl. Phys. **B945**, 114662 (2019).

[10] J.-P. Lansberg, H.-S. Shao, and H.-F. Zhang, Phys. Lett. B **786**, 342 (2018).

[11] M. Butenschoen, Z.-G. He, and B. A. Kniehl, Phys. Rev. Lett. **114**, 092004 (2015).

[12] R. Aaij et al. (LHCb Collaboration), Eur. Phys. J. C **73**, 2631 (2013).

[13] N. Brambilla *et al.*, Eur. Phys. J. C **71**, 1534 (2011).
[14] H. Han, Y.-Q. Ma, C. Meng, H.-S. Shao, and K.-T. Chao, Phys. Rev. Lett. **114**, 092005 (2015).
[15] M. Butenschoen and B. A. Kniehl, Phys. Rev. Lett. **108**, 172002 (2012).
[16] K.-T. Chao, Y.-Q. Ma, H.-S. Shao, K. Wang, and Y.-J. Zhang, Phys. Rev. Lett. **108**, 242004 (2012).
[17] M. G. Echevarria, J. High Energy Phys. 10 (2019) 144.
[18] S. P. Baranov and A. V. Lipatov, Eur. Phys. J. C **79**, 621 (2019).
[19] I. Babiarz, R. Pasechnik, W. Schfer, and A. Szczurek, J. High Energy Phys. 02 (2020) 037.
[20] C. Royon, in *TeV4LHC Workshop: 2nd Meeting Brookhaven, Upton, New York, 2005* (2006), http://lss.fnal.gov/cgi-bin/find_paper.pl?conf-06-018-E.
[21] M. G. Albrow *et al.*, J. Instrum. **4**, T10001 (2009).
[22] M. Trzebiski, Acta Phys. Pol. B **46**, 1499 (2015).
[23] C. Royon (ATLAS, CMS, LHCb, and TOTEM Collaborations), EPJ Web Conf. **172**, 06007 (2018).
[24] L. A. Harland-Lang, V. A. Khoze, M. G. Ryskin, and W. J. Stirling, Int. J. Mod. Phys. A **29**, 1430031 (2014).
[25] R. S. Pasechnik, A. Szczurek, and O. V. Teryaev, Phys. Lett. B **680**, 62 (2009).
[26] R. S. Pasechnik, A. Szczurek, and O. V. Teryaev, Phys. Rev. D **78**, 014007 (2008).
[27] V. A. Khoze, A. D. Martin, M. G. Ryskin, and W. J. Stirling, Eur. Phys. J. C **35**, 211 (2004).
[28] R. S. Pasechnik, A. Szczurek, and O. V. Teryaev, Phys. Rev. D **81**, 034024 (2010).
[29] K. Akiba *et al.* (LHC Forward Physics Working Group), J. Phys. G **43**, 110201 (2016).
[30] L. A. Harland-Lang, V. A. Khoze, and M. G. Ryskin, Eur. Phys. J. C **76**, 9 (2016).
[31] M. Boonekamp, A. De Roeck, R. B. Peschanski, and C. Royon, Phys. Lett. B **550**, 93 (2002).
[32] S. N. White, Nucl. Phys. B, Proc. Suppl. **179–180**, 125 (2008).
[33] S. Abachi *et al.* (D0 Collaboration), Phys. Rev. Lett. **72**, 2332 (1994).
[34] F. Abe *et al.* (CDF Collaboration), Phys. Rev. Lett. **74**, 855 (1995).
[35] T. Aaltonen *et al.* (CDF Collaboration), Phys. Rev. D **82**, 112004 (2010).
[36] T. Aaltonen *et al.* (CDF Collaboration), Phys. Rev. D **86**, 032009 (2012).
[37] T. Affolder *et al.* (CDF Collaboration), Phys. Rev. Lett. **84**, 232 (2000).
[38] G. Ingelman and P. E. Schlein, Phys. Lett. **152B**, 256 (1985).
[39] V. P. Gonalves, L. S. Martins, and B. D. Moreira, Phys. Rev. D **96**, 074029 (2017).
[40] C. Royon, L. Schoeffel, S. Sapeta, R. B. Peschanski, and E. Sauvan, Nucl. Phys. **B781**, 1 (2007).
[41] M. Luszczak, R. Maciula, A. Szczurek, and M. Trzebinski, J. High Energy Phys. 02 (2017) 089.
[42] M. Luszczak, A. Szczurek, and C. Royon, J. High Energy Phys. 02 (2015) 098.
[43] M. uszczak, R. Maciua, and A. Szczurek, Phys. Rev. D **91**, 054024 (2015).

[44] N. I. Kochelev, T. Morii, and A. V. Vinnikov, Phys. Lett. B **457**, 202 (1999).
[45] A. Donnachie and P. V. Landshoff, Nucl. Phys. **B303**, 634 (1988).
[46] M. Rangel, C. Royon, G. Alves, J. Barreto, and R. B. Peschanski, Nucl. Phys. **B774**, 53 (2007).
[47] Q.-D. Zhou, Y. Itow, T. Sako, and H. Menjo, J. Phys. Soc. Jpn. Conf. Proc. **19**, 011041 (2018).
[48] R. Staszewski, J. Chwastowski, K. Korcyl, and M. Trzebinski, Nucl. Instrum. Methods Phys. Res., Sect. A **801**, 34 (2015).
[49] Q.-D. Zhou, Y. Itow, H. Menjo, and T. Sako, Proc. Sci., KMI2017 (**2017**) 066.
[50] O. Adriani *et al.* (LHCf Collaboration), J. Instrum. **3**, S08006 (2008).
[51] B. Abelev *et al.* (ALICE Collaboration), Eur. Phys. J. C **73**, 2456 (2013).
[52] Tichouk, H. Sun, and X. Luo, Phys. Rev. D **99**, 114026 (2019).
[53] A. Petrelli, M. Cacciari, M. Greco, F. Maltoni, and M. L. Mangano, Nucl. Phys. **B514**, 245 (1998).
[54] R. Basu and K. Sridhar, Eur. Phys. J. C **34**, 367 (2004).
[55] Z.-B. Kang, Y.-Q. Ma, and R. Venugopalan, J. High Energy Phys. 01 (2014) 056.
[56] A. Schäfer and J. Zhou, Phys. Rev. D **88**, 014008 (2013).
[57] F. Maltoni and A. D. Polosa, Phys. Rev. D **70**, 054014 (2004).
[58] P. L. Cho and A. K. Leibovich, Phys. Rev. D **53**, 6203 (1996).
[59] V. A. Khoze, A. D. Martin, and M. G. Ryskin, J. Phys. G **45**, 053002 (2018).
[60] H. Sun, Phys. Rev. D **95**, 056023 (2017).
[61] B. Muller and A. J. Schramm, Nucl. Phys. **A523**, 677 (1991).
[62] V. Guzey and M. Klasen, J. High Energy Phys. 04 (2016) 158.
[63] E. Basso, V. P. Goncalves, A. K. Kohara, and M. S. Rangel, Eur. Phys. J. C **77**, 600 (2017).
[64] E. Gotsman, H. Kowalski, E. Levin, U. Maor, and A. Prygarin, Eur. Phys. J. C **47**, 655 (2006).
[65] K. A. Olive *et al.* (Particle Data Group), Chin. Phys. C **38**, 090001 (2014).
[66] S. R. Klein, J. Nystrand, J. Seger, Y. Gorbunov, and J. Butterworth, Comput. Phys. Commun. **212**, 258 (2017).
[67] A. K. Kohara, E. Ferreira, and T. Kodama, Eur. Phys. J. C **74**, 3175 (2014).
[68] C. Marquet, D. E. Martins, A. V. Pereira, M. Rangel, and C. Royon, Phys. Lett. B **766**, 23 (2017).
[69] J. D. Bjorken, Phys. Rev. D **47**, 101 (1993).
[70] B. Kopeliovich, R. Pasechnik, and I. Potashnikova, Int. J. Mod. Phys. E **25**, 1642001 (2016).
[71] E. Gotsman, E. Levin, and U. Maor, Eur. Phys. J. C **71**, 1685 (2011).
[72] V. A. Khoze, A. D. Martin, and M. G. Ryskin, Eur. Phys. J. C **55**, 363 (2008).
[73] S. Chatrchyan *et al.* (CMS Collaboration), Phys. Rev. D **87**, 012006 (2013).
[74] G. Aad *et al.* (ATLAS Collaboration), Phys. Lett. B **754**, 214 (2016).
[75] A. Aktas *et al.* (H1 Collaboration), Eur. Phys. J. C **48**, 715 (2006).

[76] C. O. Rasmussen and T. Sjstrand, J. High Energy Phys. 02 (2016) 142.

[77] A. Aktas *et al.* (H1 Collaboration), Eur. Phys. J. C **48,** 749 (2006).

[78] A. D. Martin, W. J. Stirling, R. S. Thorne, and G. Watt, Eur. Phys. J. C **63,** 189 (2009).

[79] M. Butenschoen and B. A. Kniehl, Phys. Rev. D **84,** 051501 (2011).

[80] G.-M. Yu, Y.-B. Cai, Y.-D. Li, and J.-S. Wang, Phys. Rev. C **95,** 014905 (2017); **95,** 069901(A) (2017).

[81] V. P. Gonalves, Phys. Rev. D **88,** 054025 (2013).

[82] H.-Y. Bi, R.-Y. Zhang, H.-Y. Han, Y. Jiang, and X.-G. Wu, Phys. Rev. D **95,** 034019 (2017).

[83] A. B. Kaidalov, V. A. Khoze, A. D. Martin, and M. G. Ryskin, Eur. Phys. J. C **31,** 387 (2003).

[84] C. Royon, L. Schoeffel, R. B. Peschanski, and E. Sauvan, Nucl. Phys. **B746,** 15 (2006).

[85] O. Kepka and C. Royon, Phys. Rev. D **76,** 034012 (2007).

[86] G. Aad *et al.* (ATLAS Collaboration), Eur. Phys. J. C **72,** 1926 (2012).